Available online at www.sciencedirect.com
ScienceDirect
Acta Materialia 55 (2007) 3555–3562
Acta MATERIALIA
www.elsevier.com/locate/actamat

Influence of surface-roughness on indentation size effect

Ju-Young Kim [a], Seung-Kyun Kang [a], Jung-Jun Lee [a], Jae-il Jang [b,*], Yun-Hee Lee [c], Dongil Kwon [a]

[a] Department of Materials Science and Engineering, Seoul National University, Seoul 151-744, Republic of Korea
[b] Division of Materials Science and Engineering, Hanyang University, Seoul 133-791, Republic of Korea
[c] Division of Metrology for Quality Life, Korea Research Institute of Standards and Science, Daejeon 305-340, Republic of Korea

Received 23 January 2007; received in revised form 4 February 2007; accepted 5 February 2007
Available online 28 March 2007

Abstract

During nanoindentation of a material with a naturally rough-surface, a flattening of the rough-surface is additionally accomplished compared to nanoindentation on a flat surface. By separating analytically the work expended to flatten the rough-surface and to deform the flattened surface, we develop here a new rough-surface indentation size effect (ISE) model. This new model is applied to nanoindentation results for three Ni samples of different surface-roughness and the applicability of the model is discussed in terms of a critical contact depth for the surface-roughness effect on ISE.

Keywords: Hardness; Indentation size effect; Nanoindentation; Surface-roughness

1. Introduction

Over the past decades, advances in nanoindentation techniques along with the development of commercial equipment have made it possible to explore the mechanical properties and behavior of very small volumes of material, as reviewed by several researchers [1–7]. From extensive research through nanoindentation experiments, it is now generally accepted that the indentation hardness measured even with a geometrically self-similar pyramidal indenter (e.g., the commonly used Berkovich indenter) increases with decreasing indentation depth or force, which is the so-called indentation size effect (ISE) [8–31].

Based on Ashby's suggestion that geometrically necessary dislocations (GNDs) would increase the strength in bending or flat-punch indentation [32], many early works on the ISE [8–11] proposed a possible relationship between the GNDs and the ISE. In 1998, the most popular mechanism-based model of the ISE phenomena was established by Nix and Gao [12], who considered the density of GNDs generated by a geometrically self-similar sharp indenter together with a Taylor's dislocation model [33]. In the Nix–Gao model, the relation between the indentation hardness (H) and the indentation depth (h) can be simply described as:

$$\frac{H}{H_0} = \sqrt{1 + \frac{h^*}{h}}, \tag{1}$$

where h^* is a characteristic length depending on both the indented material and the indenter angle and H_0 is the macroscopic indentation hardness (when h is much greater than h^*). Since the linear relation between $(H)^2$ and $(1/h)$ in Eq. (1) successfully predicted the experimental indentation hardness data, the Nix–Gao model has been applied extensively (sometimes with minor revisions) and Swadener et al. extended it to a spherical indenter by assuming a parabolic geometry of the indenter [19].

However, it has been found from further research that at very shallow indentation depth (typically <100 nm), nanoindentation hardness data can deviate significantly from the predictions of the Nix–Gao model. It was suggested that this deviation at small indentation depths might be due to the inherent response of materials during nanoindentation

* Corresponding author.
E-mail address: jijang@hanyang.ac.kr (J.-i. Jang).

1359-6454/$30.00
doi:10.1016/j.actamat.2007.02.006

(Peierls stress, storage volume for GNDs and so on [17,23,28]) as well as several extrinsic factors such as blunt tip on a sharp indenter, surface-roughness, oxide layer, chemical contamination and work-hardened layers [16,22,26]. Among the extrinsic factors, some degree of surface-roughness is almost unavoidable in nanoindentation experiments [34] and thus has been of interest. Bobji and Biswas [35] demonstrated via computational simulations that surface-roughness has a significant effect on hardness. Gerberich et al. [36] divided the work done by an applied indentation force into surface work and volume work and included the surface-roughness effect in the surface work. Most recently, Zhang et al. [24] modified Eq. (1) of the Nix–Gao model and clearly demonstrated the effect of surface-roughness on the ISE by assuming flattening of the indented rough-surface by fully plastic deformations:

$$H = H_0\sqrt{1+\frac{h^*}{h}} + \frac{2e_c + gf_s}{h}, \tag{2}$$

where e_c is the dissipation energy per contact area due to plastic deformation, g is a geometric constant and f_s is the thermodynamic surface stress. However, from a practical viewpoint, some difficulties can arise in applying this bearing ratio model because e_c and f_s are hard to measure experimentally. It is thus still desirable to derive a more easily applicable relation between surface-roughness and ISE.

With this in mind, here we propose a new rough-surface ISE model. During nanoindentation, it is plausible that the material surface in contact with the indenter, regardless of its original roughness, becomes topographically smooth. Thus, material deformation by nanoindentation is accomplished by the combination of two simpler procedures: flattening of the indented rough-surface and deformation by nanoindentation of the flattened surface. The dissipated work terms for each step were derived analytically and their ratios are presented with the contact depth and ISE characteristic values. Based on the separation of the dissipated work terms, a new rough-surface ISE model is developed and its validity is experimentally examined. Our ultimate goal is to characterize the ISE by interpreting the nanoindentation hardness at shallow depths excluding the surface-roughness effect, which may be a principal extrinsic ISE factor.

2. Experiments

The surfaces of three 99.99% pure Ni samples were carefully polished with 0.05, 1 and 5 μm alumina powder intentionally to control the average surface-roughness R_a. The values of R_a were measured using an XE-100 (PSIA Inc., Suwon, Korea) atomic force microscope (AFM). The scan area was 3×3 μm close to the residual indentation impression area. Nanoindentation experiments were conducted using a Triboindenter (Hysitron Inc., Minneapolis, MN) with a three-sided pyramidal Berkovich diamond indenter. The maximum indentation force P_{max} was 5 mN and the loading and unloading rate dP/dt was 300 μN/s. The change in hardness with indentation depth was measured by partial unloading at six different indentation depths. Directly after the indentation experiments, the geometrical profiles of the residual indentation impressions were measured using the Triboindenter's AFM function, from which the final pile-up height h_{pile} around the impression was determined. Since the measured h_{pile} is valid only for the final unloading, the values of h_{pile} at each partial unloading were estimated by assuming that the ratio of h_{pile} to the maximum indentation depth, h_{max}, is approximately constant and independent of indentation depth [13].

3. Results and discussion

3.1. Measurement of surface-roughness and hardness

Fig. 1 shows the typical surface morphology and the average surface-roughness, R_a, with standard deviation measured by AFM. The parallel scratches on the surface were caused by mechanical polishing: the Ni sample polished with coarser alumina powder shows the greater roughness (e.g., $R_a = 8.65 \pm 0.73$ nm and 3.22 ± 0.33 nm for 5 μm and 1 μm powder, respectively). The surfaces polished with 0.05 μm alumina powder are so close to flat ($R_a = 0.44 \pm 0.07$ nm) that they can be assumed to be flat surfaces. Note that R_a is not equivalent to the mean value of the maximum height difference between the top of peak and the bottom of valley in the surface (R_{max} designated in ISO 4287 [37]); this maximum height difference measured experimentally in the present work was several times R_a. The detailed procedure for determining R_a is described in ISO 4287 [37] (see also the authors' previous study [34]). Fig. 2 shows the statistical distributions of surface heights, which exhibit a normal distribution regardless of average surface-roughness.

Fig. 3 shows the change in hardness H ($=P_{max}/A_c$, where A_c is contact area) as the contact depth h_c increases. This contact depth h_c was derived by adding h_{pile} (measured by AFM) to the conventional contact depth in the Oliver–Pharr method [38], i.e., $h_c = h_{max} - h_d + h_{pile}$, where h_d is the elastic deflection depth. The contact area A_c was then determined by inputting this h_c into the area function obtained from preliminary nanoindentation experiments on a fused quartz standard specimen [38]. In Fig. 3, the hardness values are clearly dependent on surface-roughness at shallow contact depths (less than about 100 nm), while they are similar at larger contact depths (greater than about 100 nm). Considering the pile-up height, the indentation depth h in Eq. (1) can be replaced by the contact depth h_c defined above, i.e.,

$$\frac{H}{H_0} = \sqrt{1+\frac{h^*}{h_c}}. \tag{3}$$

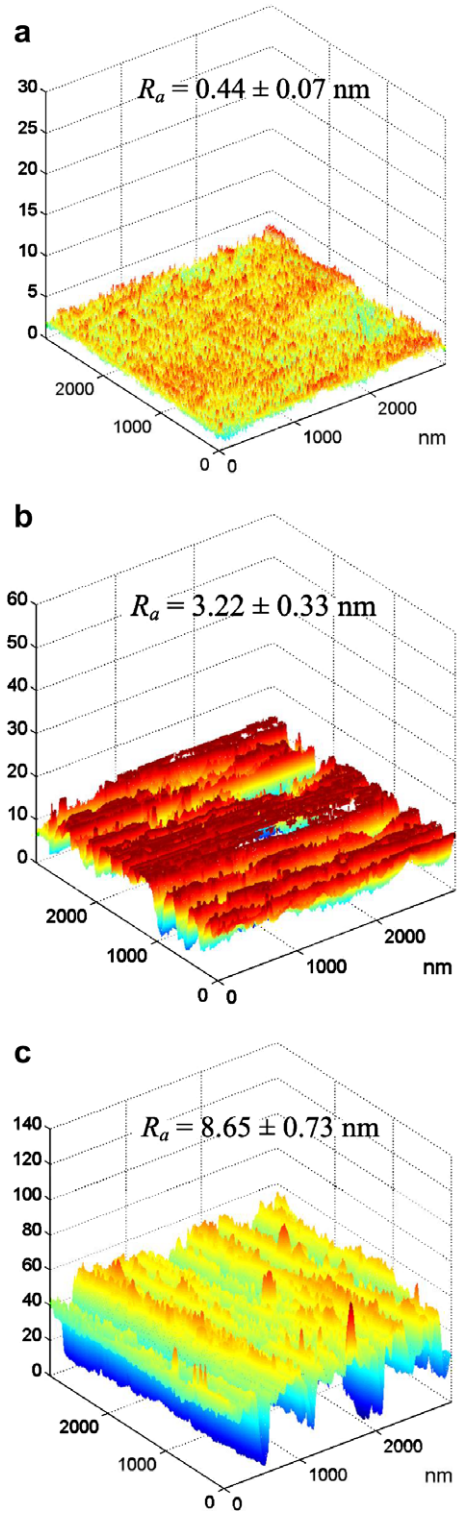

Fig. 1. Surface morphologies and average surface-roughness, R_a, measured by AFM. Scan area was 3×3 μm and specimen surfaces were mechanically polished with (a) 0.05, (b) 1 and (c) 5 μm alumina powder.

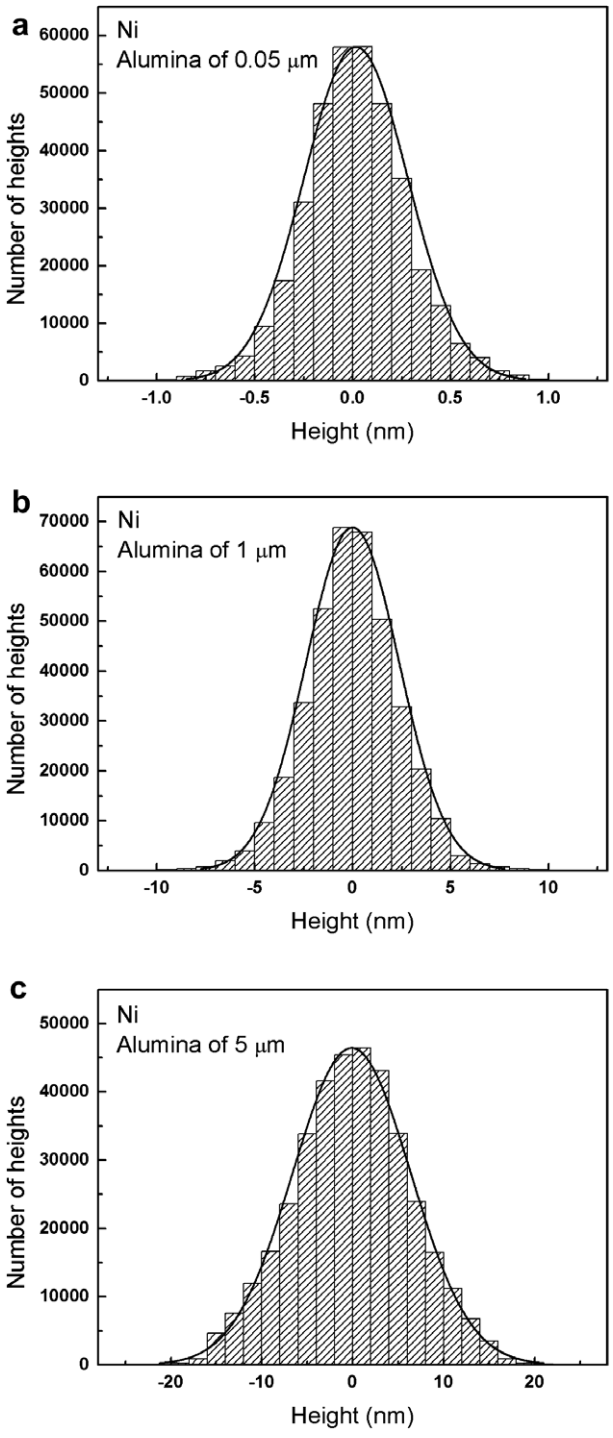

Fig. 2. Statistical distributions of surface heights for Ni samples polished with alumina powder of (a) 0.05, (b) 1 and (c) 5 μm: the mean surface heights are set to zero and the lines are curves fitted to the normal distribution functions.

Note that Eq. (3) is valid only if the original roughness of the indented surface is negligible [12]. Applying Eq. (3) to the Ni sample polished with 0.05 μm alumina powder (which had an almost flat surface, i.e., $R_a \approx 0.44$ nm) resulted in $H_0 = 1.62 \pm 0.08$ GPa and $h^* = 415.7 \pm 14.2$ nm.

3.2. Analysis of work expended for rough-surface indentation

As described above, the procedure for rough-surface indentation can be divided into two simpler steps: flattening the indented rough-surface and deformation of the flattened surface. Thus, the total work done by nanoindentation, W_{total}, can be separated into two dissipated works;

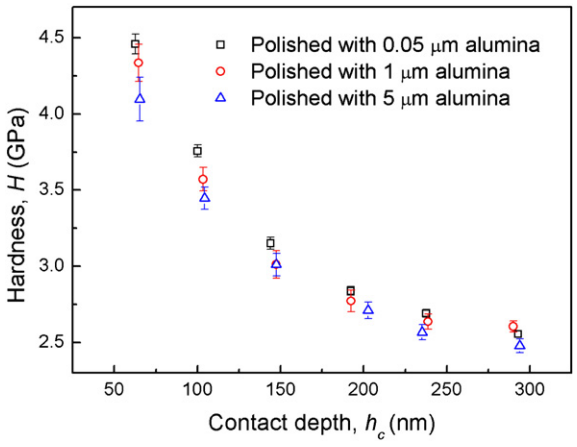

Fig. 3. Hardness vs. contact depth for Ni samples polished with 0.05, 1 and 5 μm alumina powder.

the work to flatten the rough-surface W_{rough} and that to deform the flat surface W_{flat}.

First, from the force–displacement (P–h) relations during nanoindentation, the work expended to deform the flat surface, W_{flat}, can be simply calculated as:

$$W_{\text{flat}} = \int_0^{h_c} P\,\mathrm{d}h = \int_0^{h_c} HA_c\,\mathrm{d}h = \int_0^{h_c} H \cdot \pi \tan^2\theta \cdot h^2\,\mathrm{d}h, \tag{4}$$

where θ is the half-angle of a sharp indenter (see Fig. 4). When the ISE is taken into consideration, Eq. (4) can be written as:

$$W_{\text{flat}} = \pi H_0 \tan^2\theta \cdot \int_0^{h_c} \sqrt{1+\frac{h^*}{h}} \times h^2\,\mathrm{d}h, \tag{5}$$

which after integration becomes

$$W_{\text{flat}} = \frac{\pi H_0 \tan^2\theta}{24}\left[\sqrt{h_c^2+h^*h_c}\{8h_c^2+2h^*h_c-3h^{*2}\} + 3h^{*3}\ln\left\{\sqrt{1+\frac{h_c}{h^*}}+\sqrt{\frac{h_c}{h^*}}\right\}\right]. \tag{6}$$

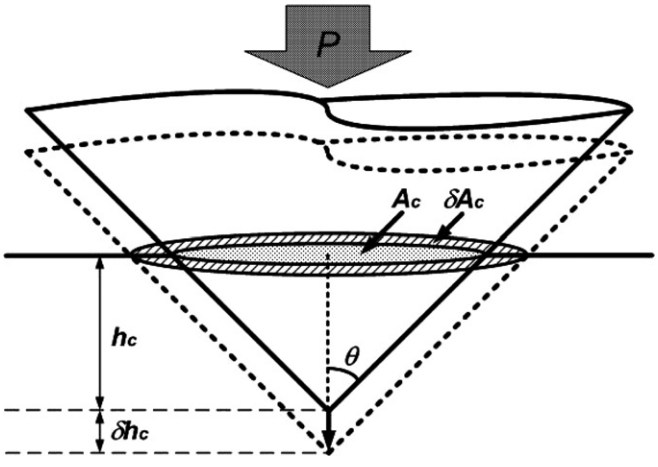

Fig. 4. Work expended to deform a flat surface by nanoindentation.

On the other hand, W_{flat} can be measured directly by integrating the loading curve in the indentation P–h curve obtained from the flat surface. Fig. 5 shows the result calculated for Eq. (6) using $H_0 = 1.62$ GPa and $h^* = 415.7$ nm obtained for Ni sample with an almost flat surface ($R_a \approx 0.44$ nm), together with the measured work values from integration of the loading curves for the same sample. The calculated value of W_{flat} is in very good agreement with the measured W_{flat}, indicating that consideration of the ISE in W_{flat} by Eq. (6) might be reasonable.

Next, we considered the work done to flatten the rough-surface W_{rough}. The flattening process is accomplished by plastic deformation of the asperities inside A_c, so that their peaks flow down to fill the valleys [24,34]. This plastic flow in a rough-surface might be easier than that for deformation by nanoindentation on a flat surface because of the free room in the neighboring valleys and thus less work per unit volume is required to flatten the rough-surface than to deform a flat surface by nanoindentation. The pressure at the onset of plastic flow, p_0, of material at a rough-surface is known to be 0.39 times H_0 [39], so that the work expended to flatten the rough-surface per unit contact area $W_{0,\text{rough}}$ becomes

$$W_{0,\text{rough}} = p_0 V_p = 0.39H_0 \cdot 0.5R_a, \tag{7}$$

where V_p is the average peak volume per unit contact area that is moved to fill up the valleys, which is 0.5 times R_a when the surface heights follow a normal distribution (as shown in Fig. 2) [24]. Using Eq. (7), the work expended to flatten the rough-surface, W_{rough}, can be determined as:

$$W_{\text{rough}} = W_{0,\text{rough}}A_c = W_{0,\text{rough}}\pi \tan^2\theta \cdot h_c^2 = 0.195\pi \tan^2\theta \cdot R_a \cdot H_0 h_c^2. \tag{8}$$

From the above results, the work ratio of W_{rough} to W_{total} ($=W_{\text{flat}} + W_{\text{rough}}$) for materials showing the ISE is given by combining Eqs. (6) and (8):

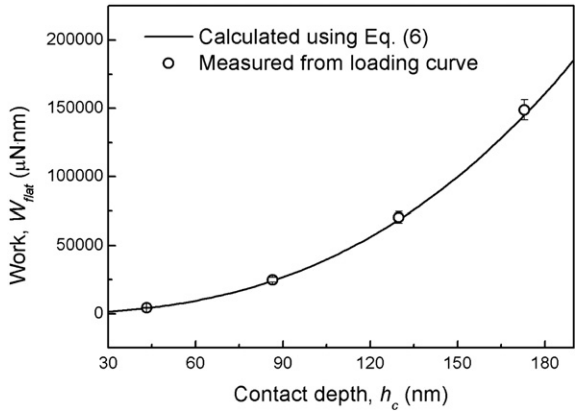

Fig. 5. Work expended to deform a flat surface by nanoindentation as calculated from Eq. (6) and as directly measured from the loading curve of Ni samples polished with 0.05 μm alumina powder.

$$\frac{W_{\text{rough}}}{W_{\text{total}}} = \frac{4.68R_a \cdot h_c^2}{\sqrt{h_c^2 + h^* h_c}\{8h_c^2 + 2h^* h_c - 3h^{*2}\} + 3h^{*3}\ln\left\{\sqrt{1+\frac{h_c}{h^*}} + \sqrt{\frac{h_c}{h^*}}\right\} + 4.68R_a \cdot h_c^2}, \quad (9)$$

which is a function of R_a, h_c, and h^*. This work ratio is shown in Fig. 6 as a function of h_c (presented as a multiple of R_a) and h^* (which increases with decreasing h_c as the usual ISE trend). The ISE characteristic length in the Nix–Gao model [12] is

$$h^* = \frac{81}{2} b\alpha^2 \cot^2\theta \cdot \left(\frac{\mu}{H_0}\right)^2, \quad (10)$$

where b is the Burgers vector, α is a geometric constant and μ is the shear modulus. Large values of H_0 (i.e., in a hard material) would cause h^* to be very small (i.e., "weak" ISE), and by Eq. (9) this would cause the work ratio ($W_{\text{rough}}/W_{\text{total}}$) to be large at a given R_a and h_c.

3.3. Development of the rough-surface ISE model

The present model begins by taking into account the possible contact morphology. During indentation, it is plausible that the material surface in contact with the indenter becomes topographically smooth, regardless of the original surface state [40]. In this case, one can say that indentation loading of increment in contact depth (δh_c) has two simpler parts: the rough-surface inside increment in the contact area (δA_c) is flattened by fully plastic deformation and the flat surface is deformed by nanoindentation. This separation is expressed by breaking down the total nanoindentation work (see Fig. 7) into

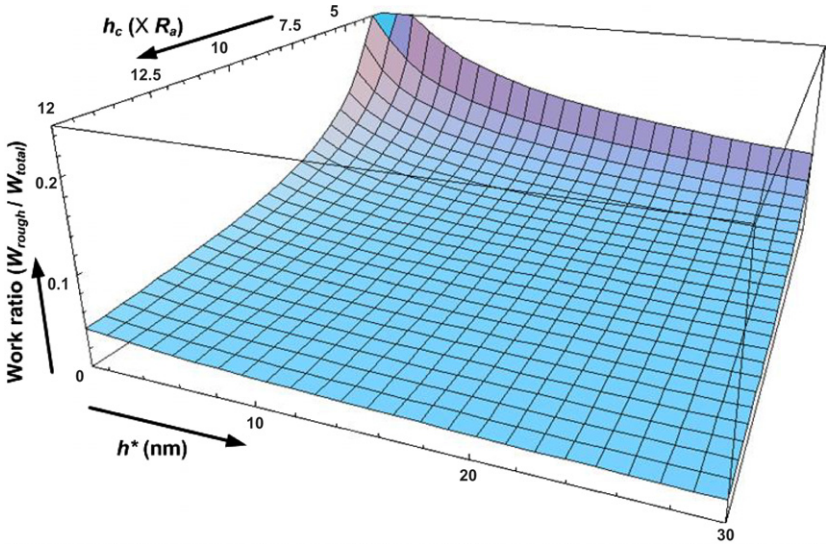

Fig. 6. Contribution of W_{rough} to W_{total}, as a function of contact depth (described as a multiple of R_a) and ISE characteristic length from Eq. (9).

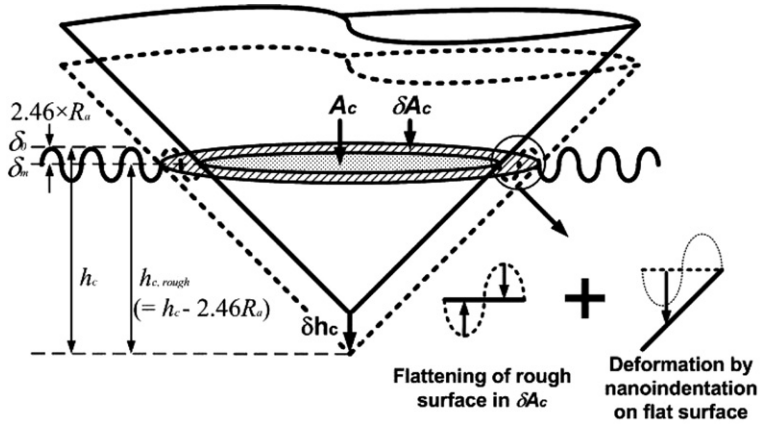

Fig. 7. Separation of nanoindentation work into work to flatten the rough-surface and work to deform the flat surface.

$$P\delta h_c = \delta W_{flat} + \delta W_{rough}, \quad (11)$$

where δW_{flat} and δW_{rough} are the infinitesimal increases in work expended to deform the flat surface and to flatten the rough-surface within δA_c, respectively. From Eqs. (8), (11) becomes

$$P\delta h_c = \delta W_{flat} + W_{0,rough}\delta A_c. \quad (12)$$

For the work expended to deform the flat surface, Eq. (3) by the Nix–Gao model [12] yields

$$P\delta h_c = \sqrt{1+\frac{h^*}{h_c}}A_c H_0 \delta h_c + W_{0,rough}\delta A_c. \quad (13)$$

By inputting $W_{0,rough} = 0.39R_a \times 0.5H_0$ (Eq. (7)) and dividing both left- and right-hand sides of Eq. (13) by $(A_c \times H_0 \times \delta h_c)$, Eq. (13) becomes

$$\frac{H}{H_0} = \sqrt{1+\frac{h^*}{h_c}} + \frac{0.39R_a}{h_c}. \quad (14)$$

In nanoindentation on a rough-surface, initial contact is likely to occur around the peak of an asperity, since the indenter tip radius is usually much greater than those of the asperities [26,41]. The height of the material surface, which is the starting point of the contact depth, is defined as the reference height. If the rough-surface inside A_c becomes smooth during indentation loading, the mean height δ_m of the original asperities, not their representative peak height, δ_0, can be taken as the reference height (Fig. 7) and the height difference between δ_m and δ_0 has been demonstrated statistically to be 2.46 times R_a [34] (i.e., $h_c|_{rough} = h_c - 2.46R_a$, where h_c is the contact depth in consideration only of the pile-up height, as mentioned above). Therefore, if this is additionally considered, Eq. (14) should be modified to become

$$\frac{H}{H_0} = \sqrt{1+\frac{h^*}{h_c - 2.46R_a}} + \frac{0.39R_a}{h_c - 2.46R_a}. \quad (15)$$

Collectively, if one can evaluate R_a and the hardness values at various contact depths, the present surface-roughness ISE model can be easily applied to obtain the macroscopic H_0 and the ISE characteristic length h^*.

3.4. Application of the new rough-surface ISE model

Hardness results measured at various contact depths were fitted to Eq. (3), which does not take into account the effect of surface-roughness, and Eq. (15), which does take this effect into account. The macroscopic hardness H_0 and the ISE characteristic length h^* obtained from Eqs. (3) and (15) are presented in Table 1. For both models, the measured H_0 values are approximately independent of R_a (as expected from the trend of hardness change with

Table 1
Characteristic ISE values from the Nix–Gao model and the rough-surface ISE model

Material (final polishing)	H_0 (GPa)	h^* (nm) by the Nix–Gao model	h^* (nm) by the rough-surface ISE model
Ni (0.05 μm alumina)	1.62 ± 0.08	415.7 ± 14.2	411.3 ± 4.5
Ni (1 μm alumina)	1.66 ± 0.12	366.7 ± 18.3	433.7 ± 8.1
Ni (5 μm alumina)	1.69 ± 0.04	317.1 ± 15.7	386.2 ± 8.2

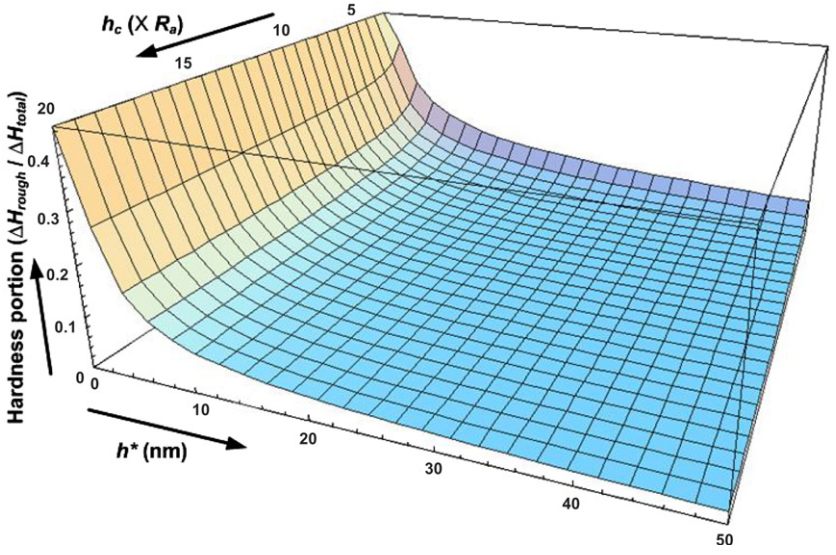

Fig. 8. Contribution of ΔH_{rough} to the total hardness increment by ISE ΔH_{total}, as a function of contact depth (as a multiple of R_a) and ISE characteristic length from Eq. (16).

contact depth seen in Fig. 3). This is not surprising since the effect of surface-roughness becomes negligible as indentation depth increases relative to a given surface-roughness. On the other hand, the influence of R_a on the h^* values is clearly different in the models. For the Nix–Gao model (Eq. (3)), the h^* values are strongly dependent on R_a; compared to the h^* value from flat surfaces, those from surfaces with $R_a \approx 3.22$ nm and $R_a \approx 8.65$ nm were underestimated by 11.8 and 23.7%, respectively. However, the value of h^* acquired from the present model does not vary significantly with R_a, despite the increasing differences in hardness values at shallow contact depths. The averages and standard deviations of the h^* values obtained from Eq. (15) were 410.4 ± 23.8 nm. This R_a-independent h^* might imply the validity of the present model, since the ISE should be insensitive to extrinsic factors such as surface-roughness.

The present model is more powerful in describing the ISE at a smaller scale (e.g., for thin films and MEMS) where the indentation depth is limited. Thus, determining the critical contact depth ($h_{c,crit}$) below which the present model is properly applicable is important. According to Eq. (15), the ISE comes from both deformation of the flat surface (the first term on the right-hand side) and that of the rough-surface (the second term on the right-hand side). This second term is the hardness increase by surface-roughness, ΔH_{rough}. The contribution of ΔH_{rough} to the total hardness increase by ISE, ΔH_{total} [$=(H - H_0)/H_0$], is given by:

$$\frac{\Delta H_{rough}}{\Delta H_{total}} = \frac{0.39R_a/(h_c - 2.46R_a)}{(H - H_0)/H_0} = \frac{0.39R_a/(h_c - 2.46R_a)}{\sqrt{1 + \frac{h^*}{h_c - 2.46R_a}} + \frac{0.39R_a}{h_c - 2.46R_a} - 1}, \quad (16)$$

which is a function of R_a, h_c and h^*. The hardness portion from surface-roughness is shown in Fig. 8 as a function of h_c (presented as a multiple of R_a) and h^*. This hardness portion increases with decreasing h_c or h^*, as did the work ratio shown in Fig. 6. However, the influence of surface roughness on hardness is more apparent than its effect on the work ratio. Note that the smaller value of $\Delta H_{rough}/\Delta H_{total}$ indicates that the effect of surface roughness on the ISE decreases. One can determine the degree of the surface-roughness effect on the ISE by an allowance limit p. At contact depths less than the critical contact depth $h_{c,crit}$, the surface-roughness effect on the ISE is greater than p and vice versa. Equating Eq. (16) to p and changing h_c to $h_{c,crit}$ yields

$$h_{c,crit} = \left(\frac{0.1521(1-p)^2}{p^2 \frac{h^*}{R_a} - 0.78p(1-p)} + 2.46 \right) R_a. \quad (17)$$

For example, if p is 0.03 (3%) for Ni with $h^* = 415.7$ nm and $R_a = 8.65$ nm, $h_{c,crit}$ is 81.48 nm. Collectively, application of the rough-surface ISE model might be especially valuable in characterizing the ISE with hardness results at contact depths less than this critical value.

4. Conclusion

We have developed a new ISE model taking into consideration surface roughness. Indentation P–h curves and hardness values at various contact depths were measured for Ni samples with different surface roughness. The total work done during nanoindentation loading, W_{total}, was separated into two dissipated works: the work expended to flatten the rough-surface, W_{rough}, and the work expended to deform the flat surface, W_{flat}. Values of W_{flat} were derived analytically and verified by comparison with those directly measured by integration of the nanoindentation loading curve obtained from an Ni sample with an almost flat surface. The value of W_{rough} was calculated and the ratio of W_{rough} to W_{total} was estimated as a function of contact depth, h_c, average surface-roughness, R_a, and the ISE characteristic length, h^*. On the basis of these dissipated works, the rough-surface ISE model was developed and applied to the nanoindentation hardness results that show variations with R_a at shallow contact depths. The value of h^* did not vary significantly with the change in R_a despite the increasing differences in hardness values at shallow contact depths. The critical contact depth was determined with an allowance limit p. The rough-surface ISE model developed here may be valuable in characterizing the ISE with nanoindentation results at contact depths less than this critical contact depth.

Acknowledgements

This research was supported partly by the Center for Nanostructured Materials Technology under the 21st Century Frontier R&D Program (Grant 06K1501-01111) of the Ministry of Science and Technology, Korea, and in part by the Standardization R&D Program (Grant 10023468) of the Ministry of Commerce, Industry and Energy, Korea.

References

[1] Oliver WC, Pharr GM. J Mater Res 2004;19:3.
[2] Cheng YT, Cheng CM. Mater Sci Eng R 2004;44:91.
[3] Nix WD. Mater Sci Eng A 1997;234–236:37.
[4] Pharr GM. Mater Sci Eng A 1998;253:151.
[5] Fischer-Cripps AC. Vacuum 2000;58:569.
[6] Mukhopadhyay NK, Paufler P. Int Mater Rev 2006;51:209.
[7] Schuh CA. Mater Today 2006;9(5):32.
[8] De Guzman MS, Neubauer G, Flinn P, Nix WD. Mater Res Soc Symp Proc 1993;308:613.
[9] Stelmashenko NA, Walls MG, Brown LM, Milman YV. Acta Metall Mater 1993;41:2855.
[10] Fleck NA, Muller GM, Ashby MF, Hutchinson JW. Acta Metall Mater 1994;42:475.
[11] Ma Q, Clarke DR. J Mater Res 1995;10:853.
[12] Nix WD, Gao H. J Mech Phys Sol 1998;46:411.
[13] McElhaney KW, Vlassak JJ, Nix WD. J Mater Res 1998;13:1300.
[14] Gao H, Huang Y, Nix WD, Hutchinson JW. J Mech Phys Sol 1999;47:1239.
[15] Huang Y, Gao H, Nix WD, Hutchinson JW. J Mech Phys Sol 2000;48:99.

[16] Liu Y, Ngan AHW. Scripta Mater 2001;44:237.
[17] Qiu X, Huang Y, Nix WD, Hwang KC, Gao H. Acta Mater 2001;49:3949.
[18] Tymiak NI, Kramer DE, Bhar DF, Wyrobek TJ, Gerberich WW. Acta Mater 2001;49:1021.
[19] Swadener JG, George EP, Pharr GM. J Mech Phys Sol 2002;50:681.
[20] Gao H, Huang Y. Scripta Mater 2003;48:113.
[21] Elmustafa AA, Stone DS. J Mech Phys Sol 2003;51:357.
[22] Qu S, Huang Y, Nix WD, Jiang H, Zhang F, Hwang KC. J Mater Res 2004;19:11.
[23] Feng G, Nix WD. Scripta Mater 2004;51:599.
[24] Zhang TY, Xu WH, Zhao MH. Acta Mater 2004;52:57.
[25] Wei Y, Wang X, Zhao M. J Mater Res 2004;19:208.
[26] Kim JY, Lee BW, Read DT, Kwon D. Scripta Mater 2005;52:353.
[27] Manika I, Maniks J. Acta Mater 2006;54:2049.
[28] Durst K, Backes B, Franke O, Göken M. Acta Mater 2006;54:2547.
[29] Qu S, Huang Y, Pharr GM, Hwang KC. Int J Plasticity 2006;22:1265.
[30] Huang Y, Zhang F, Hwang KC, Nix WD, Pharr GM, Feng G. J Mech Phys Sol 2006;54:1668.
[31] Gouldstone A, Chollacoop N, Dao M, Li J, Minor AM, Shen YL. Acta Mater, in press.
[32] Ashby MF. Phil Mag 1970;21:399.
[33] Taylor GI. Proc Roy Soc London A 1934;145:362.
[34] Kim JY, Lee JJ, Lee YH, Jang JI, Kwon D. J Mater Res 2006;21:2975.
[35] Bobji MS, Biswas SK. J Mater Res 1998;13:11.
[36] Gerberich WW, Tymiak NI, Grunlan JC, Horstemeyer MF, Baskes MI. J Appl Mech (Trans ASME) 2002;69:433.
[37] ISO standard 4287. International Organization for Standardization; 1997.
[38] Oliver WC, Pharr GM. J Mater Res 1992;7:1564.
[39] Johnson KL. Contact mechanics. Cambridge: Cambridge University Press; 1985 [chapter 13].
[40] Pullen J, Williamson JBP. Proc R Soc Lond A 1972;327:159.
[41] Bhushan B, Gupta BK. Handbook of tribology. New York: McGraw-Hill; 1991.